Dynamic Management Zones for Irrigation Scheduling

Mireia Fontanet [1,2,3], Elia Scudiero [4,5], Todd H. Skaggs[5], Daniel Fernàndez-Garcia [2,3], Francesc Ferrer [1], Gema Rodrigo [1], Joaquim Bellvert [6]

[1] LabFerrer, Cervera, 25200, Spain

[2] Department of Civil and Environmental Engineering, Universitat Politècnica de Catalunya (UPC), Barcelona, 08034, Spain

[3] Associated Unit: Hydrogeology Group (UPC-CSIC)

[4] Department of Environmental Sciences, University of California Riverside, 900 University Ave., Riverside, CA 92521, USA

[5] USDA-ARS, United States Salinity Laboratory, 450 West Big Springs Rd., Riverside, CA 92507, USA

[6] Efficient Use of Water in Agriculture Program, Institute of Agri-Food, Research and Technology (IRTA), Fruitcentre, Parc Científic i Tecnològic de Gardeny, 25008, Lleida, Spain

Highlights

- We used Sentinel 2 NDVI time-series to delineate dynamic management zones (MZ).
- Changes in MZ patterns were consistent with soil moisture spatiotemporal variability.
- Data variance fragmentation was used for daily evaluation of the dynamic MZ designs.
- Soil moisture data and model forecasts can be used to schedule MZ irrigation.

Abstract

Irrigation scheduling decision-support tools can improve water use efficiency by matching irrigation recommendations to prevailing soil and crop conditions within a season. Yet, little research is available on how to support real-time precision irrigation that varies within-season in both time and space. We investigate the integration of remotely sensed NDVI time-series, soil moisture sensor measurements, and root zone simulation forecasts for in-season delineation of dynamic management zones (MZ) and for a variable rate irrigation scheduling in order to improve irrigation scheduling and crop performance. Delineation of MZ was conducted in a 5.8-ha maize field during 2018 using Sentinel-2 NDVI time-series and an unsupervised classification. The number and spatial extent of MZs changed through the growing season. A network of soil moisture sensors was used to interpret spatiotemporal changes of the NDVI. Soil water content was a significant contributor to changes in crop vigor across MZs through the growing season. Real-time cluster validity function analysis provided in-season evaluation of the MZ design. For example, the total within-MZ daily soil moisture relative variance decreased from 85% (early vegetative stages) to below 25% (late reproductive stages). Finally, using the Hydrus-1D model, a workflow for in-season optimization of irrigation scheduling and water delivery management was tested. Data simulations indicated that crop transpiration could be optimized while reducing water applications between 11 and 28.5% across the dynamic MZs. The proposed integration of spatiotemporal crop and soil moisture data can be used to support management decisions to effectively control outputs of *crop* × *environment* × *management* interactions.

Keywords: Remote sensing; Spatial variability; Temporal variability; Precision agriculture; Soil moisture; Hydrus-1D

1. INTRODUCTION

Irrigated agriculture is essential to global food production, especially because of projected population growth (Döll, 2002). Irrigation water is commonly applied uniformly over an entire field. Yet, field soil water content is typically non-uniform because of spatial variability in soil hydraulic properties (Hawley, 1983), topography (Burt and Butcher, 1985), and vegetation growth (Le Roux et al., 1995). When field spatial variability is significant (Baveye and Laba, 2014; Thorp, 2019), differential irrigation water management that accounts for variability may improve the cost-effectiveness of irrigation (Liang et al., 2016; Martini et al., 2017) by increasing for instance water use efficiency and productivity as well as decreasing nutrient leaching.

Precision agriculture seeks to optimize farming operations via site-specific management plans that vary the application of nutrients and water across a field based on variations in soil and crop conditions (Zhang et al., 2002). Field management is prescribed over contiguous areas that have homogeneous soil properties and crop conditions. These areas are called management zones (MZ). Different clustering methods, including *k*-mean, ISODATA, and Gaussian Mixture, are available for delineating MZs based on different data sources (Galambošová et al., 2014; Martinez-Casasnovas et al., 2012; Schepers et al., 2004). Commonly, yield maps, topography, remote sensing data, and soil apparent electrical conductivity are used to delineate MZs (Bellvert et al. 2012, Liu et al., 2018; Scudiero et al., 2018; Ohana-levi et al., 2019). Recently, open access or low cost remote sensing data are being used in agriculture to obtain spatiotemporal information on biophysical parameters of vegetation (Fontanet et al., 2018).

Several researchers have defined MZs in specific fields with the goal of increasing yield and decreasing water use. Inman et al. (2008) and Schenatto et al. (2015) used NDVI and other spectral vegetation indices to delineate MZs with NDVI data and different crop indices. Liu et al. (2018)

delineated MZs based on yield and maps of different vegetation indices. Scudiero et al. (2013) argued that spatial information of soil properties known to affect plant growth should guide MZ delineation. They modeled maize yield spatial variability as a function of salinity, texture, carbon content and bulk density, using geospatial apparent soil electrical conductivity and bare soil reflectance measurements as proxies for these soil properties. A similar study was presented by Reyes et al. (2019), in which MZs were defined using information of both NDVI and soil properties. Georgi et al. (2018) developed an algorithm to delineate MZs automatically based on remote sensing data. However, one of the disadvantages of this algorithm is that it does not work properly in fields with strong time-dependent spatial patterns. All the above-mentioned studies consider MZs to be static and assume no dynamic pattern during the growing season. However, in fields where crop spatial patterns change over time, some researchers have advocated for MZ delineation to also be dynamic (Cohen et al., 2016; Evans et al., 2013; Haghverdi et al., 2015; Scudiero et al., 2018).

Soil moisture sensors constitute a vital tool for real-time monitoring of soil water content dynamics in the field. Although sensors monitor soil water content at a single point, spatial and temporal variations of soil water content and their interactions with crops can be analyzed if several sensors are installed across the field (Biswas, 2014; Biswas and Si, 2011; Huang et al., 2019; Yang et al., 2016). These measurements can provide information about the source of variability between different MZs and aid in their delineation.

In this study, we integrate crop spatial and temporal information from high-resolution remote sensing, soil water sensor data, and numerical model simulations to investigate irrigation scheduling for dynamic management zones. Specifically, we: i.) characterize the spatial and temporal dynamics of crop-soil-water relations of a maize field, ii.) delineate and evaluate

91 temporally dynamic management zones for variable rate irrigation, and iii.) provide a workflow
92 for in-season optimization of irrigation scheduling and water delivery management.
93
94 ## 2. MATERIALS AND METHODS
95 ### 2.1 Study Site
96 The study was carried out in a 5.8-ha maize (*Zea mays* L.) field located in Raïmat (Lleida,
97 Spain) (Fig.1). The study region has a typical semi-arid Mediterranean climate, with an average
98 summer temperature and rainfall of 24ºC and 45 mm. The local climate was Mediterranean, with
99 an average annual rainfall and reference evapotranspiration (ET_0) of 341 mm and 1.060 mm,
100 respectively.
101 Land use at the study site has changed over the years (Fig. A.1 of Appendix A). Originally, the
102 site was a forest where no tillage occurred. Approximately 30 years ago, the land was converted
103 to a vineyard. The topography of the field was modified, with soil being added or removed in
104 various sections, such that the site can now be regarded as having an anthropogenic soil. In 2016,
105 two years year before this study, grapevines were removed and maize was grown at the site.
106
107 ### 2.2 Sowing and Irrigation
108 All agronomic management and design at the field site was implemented by cooperators
109 without our input. The field was sectioned into four plots that were each sowed with a different
110 maize variety (Fig.1). The varieties were, from west to east: p0937 (DuPont Pioneer, Johnston,
111 IA), d6980 (DEKALB Genetics Corporation, Dekalb, IL), p1524 (DuPont Pioneer), and d6780
112 (DEKALB). All plots were sown on May 3, 2018, at a sowing density of 90000 seeds·ha^{-1}. Plants
113 started to emerge on May 12, 2018. Data from the seed companies indicated that the varieties

sowed on the west and east edges (p0937 and d6780) had a faster vegetative growth than d6980 and p1524. However, all varieties were anticipated to reach full maturity between 125 to165 days after sowing. All the varieties were harvested on September 22, 2018.

The field was irrigated with a solid set sprinkler system (Nelson Irrigation Corporation, Walla Walla, WA), with sprinklers located at a 15 x 15 m spacing. Water was delivered at a rate of 6.5 $L \cdot m^{-2} \cdot h^{-1}$. Irrigation was uniformly applied over the field with scheduling and depths determined using a crop coefficient approach (FAO56). For most of the site, irrigation ended 115 days after sowing. But, in two 0.3-ha sections at the north-east end of the site, irrigation was halted 74 days after sowing due to soil waterlogging.

2.3 Soil, Environment, and Crop Measurements

Field data were collected between May and September 2018. Soil moisture, soil and crop parameters, environmental variables, and NDVI time-series were measured. In May 2018, 33 capacitive EC-5 soil moisture sensors (METER Group, Pullman, WA, USA) were installed at 11 locations named P1, P2, …, and P11 (Fig.1). The sensors were installed at 15, 35, and 50 cm depths. Water content data were registered every 30 minutes using an EM5b data logger (METER Group). The manufacturer's generic sensor calibration was used, which has a reported accuracy ± 0.03 $cm^3 \cdot cm^{-3}$ (Campbell and Devices, 1986)

At each soil moisture station, three disturbed soil samples were collected at 0-5, 5-35, and 30-60 cm depth for organic matter (OM) and soil texture analyses. The Walkley-Black method was used to measure OM (Nelson and Sommers, 1996), whereas soil particle size distribution was measured according to the hydrometer method (Gee and Bauder, 1986). Particles were categorized into the following size classes: clay (soil particle diameter, $D < 0.002$ mm), fine silt ($0.002 < D < 0.02$ mm), coarse silt ($0.02 < D < 0.05$ mm) and sand ($0.05 < D < 2$ mm). Undisturbed soil cores

were also collected at the same locations and depths for measuring soil hydraulic properties. Saturated hydraulic conductivity was measured with a KSat device (METER Group). Soil water retention measurements were obtained using Hyprop and WP4C instruments (METER Group). The Hyprop device utilizes an evaporation method (Schelle et al., 2013) and was used to obtain retention data from 0 to -85 kPa, whereas the WP4C device implements a chilled mirror dew point technique and was used to obtain measurements down to -300 MPa. The van Genuchten equations (van Genuchten, 1980) were used to model the retention data and the soil unsaturated hydraulic conductivity. In the van Genuchten model, the Ksat parameter was set to the saturated conductivity measured with the KSat device, the saturated water content parameter (θ_s) was set to the soil porosity estimated by the Hyprop device, and the residual water content parameter (θ_r) was set to the minimum water content recorded by the WP4C device. The van Genuchten shape parameters α and n were determined by fitting the model retention function to the measured data using the RETC software package (van Genuchten et al., 1991). Principal component analysis (PCA) (Abdi and Williams, 2013; Martini et al., 2017) was used to investigate the relationships between soil texture, OM, bulk density, and hydraulic parameters. The PCA calculations were done with Statistica 12 (StatSoft Inc. Tulsa, OK, USA).

A weather station consisting of an ECRN-100 rain gauge (METER Group), a cup anemometer (Davis Instruments, Hayward, CA, USA), and PYR pyranometer and VP-4 relative humidity and temperature sensors (METER Group) was installed 150 m from the north-east corner of the field. The measured temperature, wind speed, relative humidity, and solar radiation were used to calculate daily reference evapotranspiration (ET_0) using the Penman Monteith equation as specified in FAO Irrigation and Drainage Paper No. 56 (Allen et al, 1998; hereafter "FAO56"). The estimated ET_0 was converted into daily water requirements or potential evapotranspiration

160 (ET_c) using the maize crop coefficient (k_c) from FAO56. Maximum and minimum daily
161 temperature measurements were used to calculate growing degree days (GDD) according to
162 FAO56 and to determinate reference maize growing stages (Ritchie et al., 1997).

163 Remote sensing data obtained from Sentinel 2 were used to determine normalized difference
164 vegetation index ($NDVI$) (Rouse et al., 1974),

$$NDVI = \frac{(NIR - Red)}{(NIR + Red)} \quad (1)$$

165 where NIR and Red are measured reflectance values in the near-infrared and visible red regions,
166 respectively. $NDVI$ was used to evaluate spatial variability in the field. Remote sensing data were
167 downloaded with 10-m spatial resolution every 5 days unless there was cloud coverage. The first
168 and last images downloaded were the 15th and 135th day after sowing. Remote sensing data were
169 downloaded from Google Earth Engine web page (https://earthengine.google.com).

170

171 **2.4 Management Zones Delineation**

172 NDVI was used to characterize the spatial variability of crop vigor through the growing season.
173 A k-means (also known as "fuzzy c-means") unsupervised clustering algorithm (Odeh et al., 2010)
174 was used to classify the NDVI data into temporally dynamic MZs. The Grouping Analysis tool in
175 ArcMap 10.4.1 (ESRI, Redlands, CA) was used for the MZ delineation. Anytime a new Sentinel
176 2 NDVI scene was available at the site, a new MZ scheme was delineated. Designs having 2 to 6
177 MZs were considered. The Calinski–Harabasz criterion (CHC) (Harabasz et al., 1974), Eq. (2),
178 was used to evaluate the clusters and MZ delineations and select the optimum number of MZs.
179 The CHC, also known as a pseudo F-statistic, measures the ratio of between-MZ differences and
180 within-MZ similarity. It is formulated as:

$$\mathrm{CHC} = \frac{BMZSS/(MZn-1)}{WMZSS/(N-MZn)} \quad (2)$$

where N is the number of pixels, MZn is the number of considered zones, $BMZSS$ is the between-zones sum of squares, and $WMZSS$ is the within-zone sum of squares. Large CHC values indicate high within-MZ homogeneity and between-MZ heterogeneity.

The $NDVI$ averages and maximum and minimum values within each MZ were calculated for further comparison between different MZs. MZs were not defined for the beginning of the season (0-20 day after sowing) because plants had not yet germinated or were not big enough to influence $NDVI$, and for the end of the season (beyond 130 days after sowing) because in that period the crop is in a late phenological stage and not irrigated. Differences in soil properties across MZs over time were assessed using a Kruskal-Wallis (Kruskal and Wallis, 1952) rank test (i.e., a non-parametric analysis of variance), calculated with Statistica 12.

Additionally, we considered an alternative static delineation scheme, subdividing the site into four contiguous fields corresponding to the planted maize varieties. The CHC was calculated for each available $NDVI$ scene to compare the variety-based MZ approach to the dynamic $NDVI$-based MZ delineation.

2.5 Management Zone Available Water

Soil-water status for the MZs was modeled as plant available water (AW) (Liang et al., 2016; Vellidis et al., 2016; Zurweller et al., 2019):

$$AW^j(t) = \frac{1}{Z_\mathrm{T}} \sum_m \left(\frac{\theta^{j,m}(t) - \theta_\mathrm{wp}^{j,m}}{\theta_\mathrm{fc}^{j,m} - \theta_\mathrm{wp}^{j,m}} \right) \Delta z^m \quad (3)$$

where $AW^j(t)$ is the profile average available water at monitoring station j and time t, m indexes the measurement depths, Δz^m (cm) is the depth increment associated with the moisture sensor at depth m, $Z_T = \sum \Delta z_m$ (cm) is the total soil profile depth, $\theta^{j,m}$ ($cm^3 \cdot cm^{-3}$) is soil water content, $\theta_{wp}^{j,m}$ ($cm^3 \cdot cm^{-3}$) is the wilting point (water content at -1500 kPa), and $\theta_{fc}^{j,m}$ ($cm^3 \cdot cm^{-3}$) is field capacity (determined using the simulated soil drainage method of Twarakavi et al. (2009)). The AW for a MZ was defined to be the average AW for all monitoring stations located within the MZ. Note that the MZ design changed over the growing season, so the MZ membership of some stations also changed. In addition to the CHC calculation on the $NDVI$ data, the spatiotemporal variability of AW was also used for in-season evaluation of the dynamic MZ-design. Following Fraisse et al., (2001), we calculated the daily weighted within-MZ AW variance (4),

$$S_{MZ_i}^2 = \frac{N_{S_i} N_t}{N_S N_t} \times \frac{1}{N_{S_i} N_t} \sum_{j,k} \left[AW^j(t_k) - \overline{AW_i} \right]^2 \quad (4)$$

where $S_{MZ_i}^2$ is the daily weighted AW variance within management zone i; j indicates the monitoring stations within management zone i; k indicates the measurement times during the current day; N_{S_i} is the number of stations in management zone i; $N_S(= 11)$ is the total number of stations in the field; $N_t(= 48)$ is the number of measurements per day (every 30 min), $AW^j$is defined by (3), and $\overline{AW_i}$ is the average profile AW across monitoring stations in management zone i and measurement times in the current day. The total within-zone variance is equal to the sum of the weighted within-zone variances, $S^2 = \sum_i S_{MZ_i}^2$. By comparing $S^2$with the total daily field-wide AW variance, it is possible to determine how much was gained in terms of AW uniformity by dividing the field into MZs (Fraisse et al., 2001).

3. RESULTS AND DISCUSSION

220 ### 3.1 Soil Properties

221 Soil texture, organic matter (OM) content and bulk density (ρ_b) values measured at each station
222 are reported in Table 1. The soil texture classes (USDA system) of samples taken from the 11
223 locations were clay loam (42.4 % of samples), loam (42.4%), and silty clay loam (15.2%).
224 Locations on the east side (P1, P6, P7, P11) of the field had, on average, lower sand and higher silt
225 and clay contents than those on the west side. Average OM contents ranged between 0.57 and 1.96
226 %, which is typical for agricultural soils in this region (Romanyà and Rovira, 2011). Fitted and
227 measured parameters for the soil hydraulic properties at each station are reported in Table 2.
228 Consistent with the spatial trend in soil texture noted previously, the SWRCs measured on the east
229 side of the study site (stations P1, P6, P7, P11) had lower fitted n values than in the rest of the site.
230 On the wet end of a retention curve, a lower n value corresponds to a more gradual transition in
231 water content as pressure head changes. Figure A.2 of Appendix A compares SWRCs observed at
232 the locations on the west (P9) and east (P11) sides of the field.

233 The principal component analysis (PCA) indicated that eight principal components were
234 needed to explain 95% of the variability in the soil dataset. The first three components, PC1
235 (30.9%), PC2 (18.6%), and PC3 (15.9%), explained around two thirds of the variance in the soil
236 dataset. Particularly, PC1 indicated that clay content clustered (was positively correlated) with θ_{wp},
237 θ_{fc}, and α. The PC1 also indicated that clay content was negatively correlated with sand content,
238 θ_r, and n. Further detail about PC1, PC2, and PC3 are reported in Fig. A.3 of Appendix A.

239

240 ### 3.2 Remote Sensing and Dynamic Management Zones Delineation

241 The site average, minimum, and maximum $NDVI$ values for each available Sentinel 2 scene
242 are reported in Fig. 2a. Changes in averaged $NDVI$ generally corresponded to the evolution of ET_c

243 at the site, consistent with reports for maize grown in Mediterranean climates in other studies
244 (Segovia-Cardozo et al., 2019; Toureiro et al., 2017). Figure 2b shows that cumulative input water
245 (irrigation and precipitation) (618 mm) exceeded by 10.2% the site-wide cumulative ET_c (561
246 mm). At the bottom of Fig. 2, reference growing stages for maize at the site are shown (Ritchie et
247 al., 1997). Varieties needed between 120 and 130 days to reach maturity. Thus, we considered the
248 reference growing stages to be representative for all maize varieties grown at the site. $NDVI$ and
249 ET_c were low during the early vegetative stages, had maximum values during the late vegetative
250 stage (VT) through the beginning of the reproductive stages (R1-R6), then decreased after R6. The
251 temporal changes of $NDVI$ at the site are comparable to those observed in other studies on maize
252 (Viña et al., 2004). In the early vegetative stages (V0 to V5), the $NDVI$ range of each Sentinel 2
253 scene was narrow. In later vegetative stages and early reproductive stages, the $NDVI$ ranges were
254 much larger, indicating considerable variability in crop status (greenness, health) at the site.
255 Figure 3a shows the spatiotemporal changes of $NDVI$ at the sites. Areas with high and low
256 $NDVI$ were observed at the site throughout the growing season. However, the $NDVI$ spatial
257 patterns changed over time, suggesting that homogeneous or static site-specific irrigation
258 management may be inadequate to address crop needs over time at this site. Figure 3b shows the
259 dynamic MZ delineation obtained with unsupervised clustering of the $NDVI$ data. The number of
260 MZ and its spatial distribution changed throughout the growing season. At the beginning of the
261 season, until 50 days after sowing, it seems that the optimal number of homogeneous MZ was
262 three. The MZ1 covered the north-west side of the site and had the highest $NDVI$ values; the MZ2
263 had intermediate $NDVI$ and spanned across the south of the site until the 45th day after sowing and
264 after that over the south-west only. The MZ3 had lower $NDVI$ values and was initially the north-
265 eastern side of the site, then covered the entire western side of the field at 45 days after sowing.

From the 50th day after sowing, the CHC indicated that four clusters were best at identifying areas with homogeneous $NDVI$. MZ1 and MZ2 remained relatively similar to their early season delineations. The MZ4 identified an area of moderately low $NDVI$ at the south-eastern portion of the site, whereas MZ3, on the north-eastern side of the site, was characterized by the lowest $NDVI$ values. The spatial patterns of the four MZs changed only slightly over time, until the 130th day after sowing, when the size of MZ3 increased remarkably while MZ4 decreased. The unsupervised $NDVI$ clustering was compared to dividing the site into four blocks, one for each maize variety. Figure 3c shows the CHC values for $NDVI$ clustering into dynamic MZ and into varietal-based blocks through the growing season. The dynamic MZ-design strategy had larger CHC values for the entire growing season than the variety-block strategy, indicating that the dynamic MZs identified by unsupervised clustering had more homogeneous $NDVI$ than the varietal blocks.

Figure 3a shows contrasting $NDVI$ values between the eastern and western side of the field, especially visible along the boundary between the d6980 and p1524 varieties. The boundary between the d6980 and p1524 varieties seemed to be a big factor in the determination of the boundary between eastern (MZ1 and MZ2) and western (MZ3 and MZ4) zones from 55 to 120 days after sowing (Fig. 3b). Figure A.1.f of Appendix A shows the p1524 and d6780 varieties doing relatively poorly in July 2018. Therefore, in addition to different soil hydraulic properties on the east side of the field, crop genetics (e.g., pest resistance, germination rate between the varieties) and uneven management (e.g., mechanical sowing, fertilization, soil tillage) could have been contributing factors to the poor performance of the p1524 and d6780 varieties. Changes in MZ delineation over time led to some changes in MZ membership for certain soil-water monitoring stations (Table 3). These changes occurred frequently in the early vegetative stages

289 (until 54 days after sowing). No MZ membership change occurred in the late vegetative and
290 reproductive stages. The MZs were characterized by contrasting soil properties throughout the
291 season. The MZ had significantly ($p<0.05$) different PC1 scores throughout the season according
292 to the Kruskal Wallis test: MZ1 and MZ2 were characterized by low PC1 scores, whereas MZ3
293 and MZ4 were characterized by the highest PC1 scores (Fig. A.3 of Appendix A).
294

295 **3.3 NDVI and Water Applied**

296 Changes in $NDVI$ and AW across MZs are depicted in Fig. 4a (MZ1), 4b (MZ2), 4c (MZ3),
297 and 4d (MZ4). Through the growing season, $NDVI$ in MZ1 and MZ2 was higher than in MZ3 and
298 MZ4. Furthermore, $NDVI$ was slightly higher in MZ1 than in MZ2. Average AW in MZ1 was
299 close to 1 (i.e., water content was near θ_{fc}) throughout the entire growing season. Average AW in
300 MZ2 was greater than 1 at the beginning of the season (until 45 days after sowing) and then very
301 close to 1 through the end of the growing season. Portions of MZ3 and MZ4 had lower $NDVI$
302 values than MZ1 and MZ2. In these areas, irrigation was likely excessive. AW was considerably
303 higher than 1 for the entire vegetative growth of maize and during the early reproductive stages.
304 Once irrigation was halted in the northeastern corner of the site (i.e., approximately over the area
305 comprised by MZ3) at 74 days after sowing, the AW in MZ3 gradually decreased until the end of
306 the season, while $NDVI$ in MZ3 remained stable. Halting irrigation in the northeastern corner of
307 the site had little-to-no effect on the spatial extent of MZ3 and the other MZs, as shown in Fig.
308 3c.The analysis of the daily total within-MZ AW variance (S^2) provided further support for the
309 use of $NDVI$ to identify areas with similar AW conditions at the site. In Fig. 4e, the calculated total
310 MZ variance is normalized by the daily whole-site AW variance. Especially beyond 45 days after
311 sowing (the beginning of the VT growth stage), the normalized within-MZ variance is much less

than 1, showing that a large part of the total AW variance was explained by splitting the site into dynamic MZs delineated based on an analysis of $NDVI$. Fraisse et al. (2001) used yield within-zone variance to evaluate soil-derived MZs at the end of the season. Our results suggest that daily $AW\ S^2$could also be used for in-season evaluation of management zone designs.

The AW and $NDVI$ time series data show that soil water content was a major factor determining $NDVI$ spatiotemporal variability at the site. $NDVI$ is an indicator of the canopy vegetative growth, and several studies have found positive correlations between $NDVI$, AW, and canopy vigor in different crops (Scudiero et al., 2014; West et al., 2018). However, those studies were for water scarce conditions. It is well known that crop water stress and reductions in canopy growth can occur to either deficit of water (i.e. drought) or excess of water (i.e. flooding) (Feddes et al., 1978). In the current study, where maize was grown under nearly waterlogged conditions for most of the growing season (Fig. 4), changes in $NDVI$ and AW between consecutive Sentinel 2 scenes were negatively correlated, with Pearson r equal to -0.64 (MZ1), -0.87 (MZ2), -0.79 (MZ3), and -0.83 (MZ4) (all significant at $p<0.05$). Thus, as reported in different studies (Long et al., 2015; Quebrajo et al., 2018; Scudiero et al., 2018; Shanahan et al., 2008), $NDVI$ data alone should not be used to make irrigation management decisions; $NDVI$ (and/or other plant canopy information) should be integrated with soil information to properly understand plant processes at a site.

3.4 Irrigation Scheduling Simulations

With respect to within-season management decisions, one way to make a connection between $NDVI$-based dynamic management zone delineation and soil conditions would be to use a simulation model to make within-season forecasts of soil and crop conditions for different

335 management options. Several authors have simulated different irrigation strategies, for different
336 purposes, in order to define the most appropriate irrigation strategy (Autovino et al., 2018; Haj-
337 Amor and Bouri, 2020; Sakaguchi et al., 2019). In the remainder of this paper, we determine a
338 hypothetical optimal irrigation schedule for each growing stage using the simulation/optimization
339 approach developed by Fontanet (2019).We first show that a physically based simulation model,
340 Hydrus-1D (Šimůnek et al., 2016), is consistent with NDVI-based zoning by simulating the field
341 experiment and demonstrating agreement between measured AW and simulated available water
342 (SAW), as well as showing a correspondence between simulated transpiration (ST_a) rates and
343 $NDVI$. Next, we use the calibrated model to investigate what-if irrigation scenarios, calculating a
344 hypothetical irrigation scheduling table for each dynamic MZ that could have been generated from
345 NDVI within season to guide irrigation.
346
347 **3.4.1 Hydrus 1-D available water and transpiration simulations**
348 The well-known Hydrus-1D model solves the Richards Equation numerically to simulate
349 variably saturated water flow and root water uptake in soils. The model inputs and
350 parameterizations used in our simulations are detailed in Appendix B. Simulations of the
351 experiment for differing monitoring locations all used the same inputs and parameters except for
352 (i.) the soil hydraulic properties, which were measured at each station during the field campaign
353 (Table 2), and (ii.) the irrigation boundary condition, which differed only for stations P10 and P11
354 because irrigation was stopped during the experiment.
355 In Fig. 5, daily observed AW for each station is compared with daily-simulated available water
356 (SAW). Generally good agreement between AW and SAW existed for all stations, although it is
357 acknowledged that the AW time courses were relatively non-dynamic. Still, the simulations were

done using independently measured hydraulic properties and without any calibration, so the agreement is quite good (modeling details can be found in Appendix B). Missing data towards the end of the season in P7 was due to rodents chewing on the sensor cables.

Figure 6 shows the weekly-simulated actual transpiration (ST_a) at each MZ and the potential transpiration (T_p) at the site. At MZ1 and MZ2, ST_a weekly averages were always equal or near the potential transpiration. At MZ3 and MZ4, ST_a weekly values were remarkably lower than the potential. There was good correspondence between ST_a and $NDVI$ at each MZ, with a Pearson *r* of 0.6 (MZ1), 0.51 (MZ2), 0.69 (MZ3), and 0.82 (MZ4). In agreement with the results discussed for $NDVI$ and AW data (section *3.2. Remote Sensing and Dynamic Management Zones Delineation*), low ST_a values at MZ3 and MZ4 were due to waterlogging (root water uptake and transpiration is reduced in the model whenever simulated soil water content exceeds a threshold value; see Appendix B). Stations in MZ3 and MZ4 (see Table 3) had AW and SAW over 1 for most of the growing season (Fig. 4).

3.4.2 Irrigation scheduling for within-season decision making

We adopted the method of Fontanet (2019) to investigate optimal irrigation scheduling for dynamic MZs In this method, irrigation of duration τ [T] is prescribed whenever the soil moisture content decreases below a critical threshold level ($\boldsymbol{h_{th}}$) as indicated by readings from a soil water pressure head sensor(s). The irrigation rate is assumed to be a fixed constant for a given irrigation system. The recommended duration and threshold are determined using a simulation/optimization procedure. Simulations are made using forecasted daily or weekly crop water demand (reference ET_0) and a range of values for the irrigation scheduling parameters, $\boldsymbol{h_{th}}$ and τ. The optimal parameter values are those that maximize seasonal transpiration in the simulations (transpiration

being, for many agronomically important crops, proportional to marketable yield). In adapting the simulation/optimization method, we make separate recommendations for each MZ, and update them whenever there is a change in MZ station membership. The recommended values of $\boldsymbol{h_{th}}$ and τ for a given MZ are the average values determined for monitoring stations within the zone. For simplicity, we use in this example the known daily potential ET_0 for the forecasted model boundary condition (rather than historical data which would be necessary for actual within-season forecasts). Haghverdi et al. (2015) and Liang et al. (2016) proposed calculating crop water requirements as a function of root growth since the soil depth to refill increases as roots grow deeper. Similarly, in our simulations, we triggered irrigation based on readings from progressively deeper sensors as the season progressed. In principle, when multiple sensor depths are available, the sensor depth could be treated as an additional optimization parameter. Full details on our implementation of the Fontanet, (2019) procedure are given in Appendix C.

Although the Fontanet (2019) method prescribes an optimized irrigation schedule, in practice a grower may not be able to irrigate exactly according to a schedule and sensor readings, particularly when there are multiple management zones. Therefore, we also calculated recommended irrigation durations (or, equivalently, irrigation amounts) for soils that have become dryer than the "optimal" irrigation trigger point.

The resulting irrigation scheduling calendar for dynamic-MZ irrigation is presented in Table 4. Optimal irrigation strategies for each growth stage are shown in bold. The other table entries show irrigation recommendations for field sections that are dryer than the optimal trigger point. Across all MZs, the optimal irrigation durations were in the range of 1.9 to 2.6 h. However, the triggering thresholds varied by location. Thresholds for MZ1 and MZ2 were in the range of -18.3 to -30 kPa, whereas the range for MZ3 and MZ4 was -10 to -20 kPa. In general, the

404 recommendations are for more frequent and slightly shorter irrigations in MZ3 and MZ4, which
405 are located on the east side of the field and feature finer textured soils. With the specific Hydrus-
406 1D model parameterization used in the current study, uptake and transpiration are penalized
407 whenever any portion of the soil approaches saturation. The recommendation
408 of somewhat shorter, more frequent irrigations on the east side is due to optimization's aversion
409 to creating overly wet soil conditions near the surface, such as may occur (albeit briefly) during a
410 longer irrigation.

411 Table 5 compares seasonal transpiration and irrigation simulated with optimal scheduling
412 versus the amounts obtained simulating the field experiment. For MZ1 and MZ2, the optimal
413 schedule recommended 11 to 13 % less water and increased transpiration by 5 to 8 %. For MZ3,
414 29 % less water was recommended, with an increase in transpiration of 24 %. And for MZ4, a 17
415 % reduction in irrigation corresponded to a massive 53% increase in transpiration. These results
416 are consistent with our earlier findings and discussion indicating the field was over-irrigated,
417 especially in MZ3 and MZ4.

418

419 **4. CONCLUSIONS**

420 Irrigation scheduling is complicated due to the spatial and temporal variability of a number of
421 variables and parameters. In this work, we investigated a workflow for improved precision
422 irrigation scheduling using data from a field where four maize varieties were sown. The workflow
423 is based on dynamic MZ delineation with unsupervised $NDVI$ clustering. This study demonstrates
424 that delineation of MZs based on NDVI clustering was able to statistically represent within-field
425 spatial variability better than delineating MZs only based on maize varieties. Additionally, the
426 optimal number and spatial configuration of the MZs were found to change over the growing

427 season. The highest number of MZs was four. The MZ1 and MZ2 corresponded to field sections
428 where NDVI values reflected a typical maize crop performance, whereas MZ3 and MZ4 featured
429 relatively low $NDVI$ values indicative of poor maize growth.

430 Soil water content showed that the variation in crop performance was attributable to soil
431 hydraulic properties, soil available water, and over-irrigation. Further, a relationship existed
432 between NDVI and soil available water. The results indicated that soil available water could
433 potentially also be used for, or incorporated into, in-season evaluation of management zone
434 designs.

435 Lastly, we proposed a method of combining dynamic management zone delineation with
436 Hydrus 1-D model forecasts for irrigation scheduling. The field experiment was first simulated to
437 confirm the model parameterization and demonstrate its consistency with the obtained NDVI and
438 soil water content data. We then used model simulations to determine an optimal zonation and
439 irrigation calendar for different crop growth stages that could have been generated and updated in
440 real time during the season. Simulations with the optimized irrigation schedule produced an
441 increase in transpiration and a decrease in water use as compared to the field trial (which, again,
442 was over-irrigated). The improvement was especially remarkable for MZ3 and MZ4, where
443 irrigation was reduced by 28.5 and 16.6 %, and transpiration increased by 23.9 and 52.6 %,
444 respectively.

445 In summary, we note that although NDVI is useful for dynamically delineating management
446 zones, for irrigation scheduling it is recommended that NDVI be combined with some additional
447 measure of soil conditions. Low NDVI values may be indicative of poor crop performance, but
448 without other information it is not possible to determine the cause nor recommend a remedial
449 irrigation or management practice.

Appendix A. Supplementary figures

Supplementary material related to this article can be found, in the online version, at doi: #

Appendix B. Hydrus -1D Simulations

Hydrus-1D (Šimůnek et al., 2016, 2008) was used to simulated soil moisture dynamics and water balance components at each monitoring station. Each simulation spanned 105 days, from the 18th to the 123rd day after sowing. The 60 cm soil profile consisted of three layers/materials, as specified in Table 2. Soil hydraulic properties were specified using the van Genuchten-Mualem model (van Genuchten, 1980) as follows:

$$\theta(h) = \begin{cases} \theta_r + \dfrac{\theta_s - \theta_r}{(1 + |\alpha h|^n)^m} & h < 0 \\ \theta_s & h \geq 0 \end{cases} \quad \text{(B.1)}$$

and

$$K(h) = K_s S_e^{1/2} \left[1 - \left(1 - S_e^{1/m}\right)^m\right]^2, \quad \text{(B.2)}$$

where θ ($cm^3 \cdot cm^{-3}$) is the volumetric water content; h is the soil water pressure head (cm); θ_s ($cm^3 \cdot cm^{-3}$) is saturated water content; θ_r ($cm^3 \cdot cm^{-3}$) is residual water content; K_s ($cm \cdot d^{-1}$) is saturated hydraulic conductivity; n and α are shape parameters; $S_e = \frac{\theta - \theta_r}{\theta_s - \theta_r}$; and $m = 1 - 1/n$.

In Hydrus, root water uptake is simulated using a sink term S which has three parts, the potential transpiration rate (T_p) ($cm \cdot d^{-1}$), the root density distribution (β) (cm^{-1}), and the dimensionless water stress function ($\alpha(h)$):

$$S(h, z, t) = \alpha(h, z, t)\beta(z, t)T_p(t) \quad \text{(B.3)}$$

The actual transpiration rate (T_a) ($cm \cdot d^{-1}$) is calculated by integrating Eq. (B.3) over the root zone

468 L_R:

$$T_a = \int_{L_R} S(h,z,t)dz = T_p \int_{L_R} \alpha(h,z,t)\beta(z,t)dz \quad \text{(B.4)}$$

469 Root depth was measured twice a month during the field campaign at P9 station. This
470 information was used to parameterize the Hydrus root growth module.

471 Water stress ($\alpha(h)$) was modeled using the Feddes et al. (1978) function:

$$\alpha(h) = \begin{cases} \dfrac{h-h_4}{h_3-h_4} & h_3 > h > h_4 \\ 1 & h_2 \geq h \geq h_3 \\ \dfrac{h-h_1}{h_2-h_1} & h_1 > h > h_2 \\ 0 & h \leq h_4 \; or \; h \geq h_1 \end{cases} \quad \text{(B.5)}$$

472 Parameterized by four critical values of pressure head, Eq. (B.5) defines maximal uptake ($\alpha = 1$)
473 when the soil water pressure head is $h_2 \geq h \geq h_3$. Water uptake decreases linearly above or below
474 that range ($h_3 > h > h_4$ or $h_1 > h > h_2$). And uptake is zero when $h \leq h_4$ or $h \geq h_1$. According
475 to the Hydrus-1D database, the parameter values for maize are h_1 = -1.5, h_2 = -3.0, h_3 = -60. and
476 h_4 = -800. kPa, respectively. The value of h_3 was allowed to vary as a function of evaporative
477 demand as modeled by Hyrdurs-1D.
478 Three observation nodes were inserted in the domain at the same depths as the soil moisture
479 sensors, 15, 35 and 50 cm. Soil moisture values simulated at the observation nodes were used to
480 determine the simulated available water (SAW), using the same procedure as with the field data.
481 The potential evaporation and transpiration rates were calculated by partitioning ET_c into potential
482 evaporation (E_p) and transpiration (T_p) based on the canopy cover fraction (α) according to Raes
483 et al. (2009). An atmospheric boundary condition was imposed at the surface and a free drainage
484 condition was used at the bottom. Simulated actual transpiration (ST_a) and simulated applied

485 irrigation (SAI) results from each station were extracted. ST_a and SAI were calculated by averaging
486 stations located with the dynamic MZs.
487
488 **Appendix C. Irrigation Scheduling**
489 Irrigation scheduling was optimized using the methodology developed by Fontanet (2019).
490 All soil, environmental and crop inputs are the same as described previously for the Hydrus-1D
491 simulations (Appendix B). Possible values for the irrigation scheduling parameters were
492 constrained to be $h_{th} \in$ {-10, -20, …, -100 kPa} and $\tau \in$ {1, 2, 3, 4 h·d^{-1}}. The irrigation rate
493 was constant (6.5 l·h^{-1}·m^{-2}). The soil depth used to trigger irrigation (Z_{tr}) changed during the
494 growing season, becoming deeper as the season progressed. Irrigation parameters have been
495 defined at each station and at different crop growing stages (V0-V5, V6-V10, V11-V15, VT, R1-
496 R6). The optimal irrigation at each grow stage and MZ are the average values obtained for the
497 stations located in the MZ.
498
499 **Acknowledgements**
500 This study was supported by the European Commission Horizon 2020 Programme for Research
501 and Innovation (H2020) in the context of the Marie Sklodowska-Curie Research and Innovation
502 Staff Exchange (RISE) action (ACCWA project, grant agreement no.: 823965). This study was
503 also funded by the project 'Low Input Sustainable Agriculture (LISA)' under the Operational
504 program FEDER for Catalonia 2014-2020 RIS3CAT (http://www.lisaproject.cat/introduction/).

505 **Bibliography**

506 Abdi, H., Williams, L.J., 2013. Principal components analysis. Methods Mol. Biol. 930, 527–
507 547. https://doi.org/10.1007/978-1-62703-059-5_22
508 Autovino, D., Rallo, G., Provenzano, G., 2018. Predicting soil and plant water status dynamic in
509 olive orchards under different irrigation systems with Hydrus-2D: Model performance and
510 scenario analysis. Agric. Water Manag. 203, 225–235.
511 https://doi.org/10.1016/j.agwat.2018.03.015
512 Baveye, P.C., Laba, M., 2014. Moving away from the geostatistical lamppost: Why, where, and
513 how does the spatial heterogeneity of soils matter? Ecol. Modell.
514 https://doi.org/10.1016/j.ecolmodel.2014.03.018
515 Bellvert, J., Marsal, J., Mata, M., Girona, J., 2012. Identifying irrigation zones across a 7.5-ha
516 "Pinot noir" vineyard based on the variability of vine water status and multispectral images.
517 Irrig. Sci. 30, 499–509. https://doi.org/10.1007/s00271-012-0380-y
518 Biswas, A., 2014. Landscape characteristics influence the spatial pattern of soil water storage:
519 Similarity over times and at depths. Catena 116, 68–77.
520 https://doi.org/10.1016/j.catena.2013.12.004
521 Biswas, A., Si, B.C., 2011. Application of continuous wavelet transform in examining soil
522 spatial variation: A review. Math. Geosci. 43, 379–396. https://doi.org/10.1007/s11004-
523 011-9318-9
524 Burt, T.P., Butcher, D.P., 1985. Topographic controls of soil moisture distributions. J. Soil Sci.
525 36, 469–486. https://doi.org/10.1111/j.1365-2389.1985.tb00351.x
526 Campbell, C.S., Devices, D., 1986. Calibrating ECH 2 O Soil Moisture Probes 2–4.
527 Cohen, Y., Alchanatis, V., Saranga, Y., Rosenberg, O., Sela, E., Bosak, A., 2016. Mapping water

528 status based on aerial thermal imagery : comparison of methodologies for upscaling from a
529 single leaf to commercial fields. Precis. Agric. https://doi.org/10.1007/s11119-016-9484-3
530 Döll, P., 2002. Impact of climate change and variability on irrigation requirements: a global
531 prespective. Clim. Change 54, 269–293.
532 Evans, R.G., LaRue, J., Stone, K.C., King, B.A., 2013. Adoption of site-specific variable rate
533 sprinkler irrigation systems. Irrig. Sci. 31, 871–887. https://doi.org/10.1007/s00271-012-
534 0365-x
535 Feddes, R.A., Kowalik, P.J., Zaradny, H., 1978. Simulation of Field Water Use and Crop Yield.
536 Simulation Monograph 308.
537 Fontanet, M., 2019. Optimal Irrigation Scheduling Combining Water Content Sensors and
538 Remote Sensing Data. Supervisors : Daniel Fernàndez-garcia, Francesc Ferrer. Universitat
539 Politècnica de Catalunya.
540 Fontanet, M., Fernàndez-garcia, D., Ferrer, F., 2018. The value of satellite remote sensing soil
541 moisture data and the DISPATCH algorithm in irrigation fields. Hydrol. Earth Syst. Sci. 22,
542 5889–5900.
543 Fraisse, C.W., Sudduth, K.A., Kitchen, N.R., 2001. Delineation of Site-Specific management
544 Zones by Unsupervised Classification of Topographic Atributes and Soil Electrical
545 Conductivity. Am. Soc. Agric. Eng. 155 44, 155–166. https://doi.org/10.1117/12.840574
546 Galambošová, J., Rataj, V., Prokeinová, R., Prešinská, J., 2014. Determining the management
547 zones with hierarchic and non-hierarchic clustering methods 60.
548 Gee, G.W. and J.W. Bauder, 1986. Particle Size Analysis. In: Methods of Soil Analysis, Part A.
549 Klute (ed.). 2 Ed., Vol. 9 nd . Am. Soc. Agron., Madison, WI, pp: 383-411.
550 Georgi, C., Spengler, D., Itzerott, S., Kleinschmit, B., 2018. Automatic delineation algorithm for

551 site-specific management zones based on satellite remote sensing data. Precis. Agric. 19,
552 684–707. https://doi.org/10.1007/s11119-017-9549-y
553 Haghverdi, A., Leib, B.G., Washington-Allen, R.A., Ayers, P.D., Buschermohle, M.J., 2015.
554 Perspectives on delineating management zones for variable rate irrigation. Comput.
555 Electron. Agric. 117, 154–167. https://doi.org/10.1016/j.compag.2015.06.019
556 Haj-Amor, Z., Bouri, S., 2020. Use of HYDRUS-1D–GIS tool for evaluating effects of climate
557 changes on soil salinization and irrigation management. Arch. Agron. Soil Sci. 66, 193–207.
558 https://doi.org/10.1080/03650340.2019.1608438
559 Harabasz, J., Scroll, P., For, D., 1974. Communications in Statistics A dendrite method for
560 cluster analysis. Commun. Stat. 1, 37–41. https://doi.org/10.1080/03610927408827101
561 Hawley, 1983. Journal of Hydrology, 62 (1983) 179--200. J. Hydrol. 62, 179–200.
562 https://doi.org/10.1016/0022-1694(83)90102-6
563 Huang, J., Hartemink, A.E., Arriaga, F., Chaney, N.W., 2019. Unraveling location-specific and
564 time-dependent interactions between soil water content and environmental factors in
565 cropped sandy soils using Sentinel-1 and moisture probes. J. Hydrol. 575, 780–793.
566 https://doi.org/10.1016/j.jhydrol.2019.05.075
567 Inman, D., Khosla, R., Reich, R., Westfall, D.G., 2008. Normalized difference vegetation index
568 and soil color-based management zones in irrigated maize. Agron. J. 100, 60–66.
569 https://doi.org/10.2134/agronj2007.0020
570 Kruskal, W.H., Wallis, W.A., 1952. Use of Ranks in One-Criterion Variance Analysis Author (s
571): William H . Kruskal and W . Allen Wallis Published by : Taylor & Francis , Ltd . on
572 behalf of the American Statistical Association Stable URL :
573 http://www.jstor.org/stable/2280779 Accessed : 02. M J. Am. Stat. Assoc. 47, 583–621.

574 https://doi.org/10.1002/med
575 Le Roux, X., Bariac, T., Mariotti, a, 1995. Spatial partitioning of the soil water resoucre
576 between grasses and shrub compnents in a west African humid savanna. Oecologia 104,
577 145–155. https://doi.org/10.1007/BF00328579
578 Liang, X., Liakos, V., Wendroth, O., Vellidis, G., 2016. Scheduling irrigation using an approach
579 based on the van Genuchten model. Agric. Water Manag. 176, 170–179.
580 https://doi.org/10.1016/j.agwat.2016.05.030
581 Liu, H., Whiting, M.L., Ustin, S.L., Zarco-Tejada, P.J., Huffman, T., Zhang, X., 2018.
582 Maximizing the relationship of yield to site-specific management zones with object-oriented
583 segmentation of hyperspectral images. Precis. Agric. 19, 348–364.
584 https://doi.org/10.1007/s11119-017-9521-x
585 Long, D.S., Whitmus, J.D., Engel, R.E., Brester, G.W., 2015. Net returns from terrain-based
586 variable-rate nitrogen management on dryland spring wheat in Northern Montana. Agron. J.
587 107, 1055–1067. https://doi.org/10.2134/agronj14.0331
588 Martinez-Casasnovas, J.A., Agelet-Fernandez, J., Arno, J., Ramos, M.C., 2012. Analysis of
589 vineyard differential management zones and relation to vine development , grape maturity
590 and quality. Spanish J. Agric. Res. 10, 326–337.
591 Martini, E., Wollschläger, U., Musolff, A., Werban, U., Zacharias, S., 2017. Principal component
592 analysis of the spatiotemporal pattern of soil moisture and apparent electrical conductivity.
593 Vadose Zo. J. 16. https://doi.org/10.2136/vzj2016.12.0129
594 Nelson, D.W., Sommers, L.E., 1996. Total carbon, organic carbon, and organic matter. In:
595 Sparks, D.L. (Ed.), Methods of Soil Analysis: Chemical Methods, Part 3. SSSA, ASA,
596 Madison, WI, pp. 961–1010.

597 Odeh, I.O.A., McBratney, A.B., Chittleborough, D.J., 2010. Soil Pattern Recognition with
598 Fuzzy-c-means: Application to Classification and Soil-Landform Interrelationships. Soil
599 Sci. Soc. Am. J. 56, NP. https://doi.org/10.2136/sssaj1992.03615995005600020050x
600 Ohana-levi, N., Bahat, I., Peeters, A., Shtein, A., Netzer, Y., Ben-gal, A., 2019. Original papers
601 A weighted multivariate spatial clustering model to determine irrigation management zones
602 162, 719–731. https://doi.org/10.1016/j.compag.2019.05.012
603 Quebrajo, L., Perez-Ruiz, M., Pérez-Urrestarazu, L., Martínez, G., Egea, G., 2018. Linking
604 thermal imaging and soil remote sensing to enhance irrigation management of sugar beet.
605 Biosyst. Eng. 165, 77–87. https://doi.org/10.1016/j.biosystemseng.2017.08.013
606 Raes, D., Steduto, P., Hsiao, T.C., Fereres, E., 2009. AquaCrop—the FAO crop model to
607 simulate yield response to water: II. Main algorithms and software description. Agron. J.
608 101, 438–447.
609 Reyes, J., Wendroth, O., Matocha, C., Zhu, J., 2019. Delineating Site-Specific Management
610 Zones and Evaluating Soil Water Temporal Dynamics in a Farmer's Field in Kentucky.
611 Vadose Zo. J. 18, 0. https://doi.org/10.2136/vzj2018.07.0143
612 Ritchie, S.W., Hanway, J.J., Benson, G.O., 1997. How a corn plant develops.; Spec. Publ. 48.
613 Romanyà, J., Rovira, P., 2011. An appraisal of soil organic C content in Mediterranean
614 agricultural soils. Soil Use Manag. 27, 321–332. https://doi.org/10.1111/j.1475-
615 2743.2011.00346.x
616 Rouse, R.W.H., Haas, J.A.W., Deering, D.W., 1974. Monitoring Vegetation Systems in the
617 Great Plains with ERTS. Third Earth Resour. Technol. Satell. Symp. Vol. I Tech. Present.
618 NASA SP-351 309–317.
619 Sakaguchi, A., Yanai, Y., Sasaki, H., 2019. Subsurface irrigation system design for vegetable

620 production using HYDRUS-2D. Agric. Water Manag. 219, 12–18.
621 https://doi.org/10.1016/j.agwat.2019.04.003
622 Schenatto, K., Souza, E.G., Bazzi, C.L., Beneduzzi, H.M., 2015. Management Zones with NDVI
623 Data through Corn and Soybean Yield. First Conf. Prox. Sens. Support. Precis. Agric.
624 https://doi.org/10.3997/2214-4609.201413856
625 Schepers, A.R., Shanahan, J.F., Liebig, M.A., Schepers, J.S., Johnson, S.H., Luchiari, A., 2004.
626 Appropriateness of Management Zones for Characterizing Spatial Variability of Soil
627 Properties and Irrigated Corn Yields across Years. Agron. J. 96, 195–203.
628 Scudiero, E., Teatini, P., Corwin, D.L., Dal Ferro, N., Simonetti, G., Morari, F., 2014.
629 Spatiotemporal response of maize yield to edaphic and meteorological conditions in a saline
630 farmland. Agron. J. 106, 2163–2174. https://doi.org/10.2134/agronj14.0102
631 Scudiero, E., Teatini, P., Corwin, D.L., Deiana, R., Berti, A., Morari, F., 2013. Delineation of
632 site-specific management units in a saline region at the Venice Lagoon margin, Italy, using
633 soil reflectance and apparent electrical conductivity. Comput. Electron. Agric. 99, 54–64.
634 https://doi.org/10.1016/j.compag.2013.08.023
635 Scudiero, E., Teatini, P., Manoli, G., Braga, F., Skaggs, T., Morari, F., 2018. Workflow to
636 Establish Time-Specific Zones in Precision Agriculture by Spatiotemporal Integration of
637 Plant and Soil Sensing Data. Agronomy 8, 253. https://doi.org/10.3390/agronomy8110253
638 Segovia-Cardozo, D.A., Rodríguez-Sinobas, L., Zubelzu, S., 2019. Water use efficiency of corn
639 among the irrigation districts across the Duero river basin (Spain): Estimation of local crop
640 coefficients by satellite images. Agric. Water Manag. 212, 241–251.
641 https://doi.org/10.1016/j.agwat.2018.08.042
642 Shanahan, J.F., Kitchen, N.R., Raun, W.R., Schepers, J.S., 2008. Responsive in-season nitrogen

643 management for cereals. Comput. Electron. Agric. 61, 51–62.
644 https://doi.org/10.1016/j.compag.2007.06.006
645 Šimůnek, J., van Genuchten, M.T., Šejna, M., 2016. Recent Developments and Applications of
646 the HYDRUS Computer Software Packages. Vadose Zo. J. 15, 0.
647 https://doi.org/10.2136/vzj2016.04.0033
648 Šimůnek, J., van Genuchten, M.T., Šejna, M., 2008. Development and Applications of the
649 HYDRUS and STANMOD Software Packages and Related Codes. Vadose Zo. J. 7, 587.
650 https://doi.org/10.2136/vzj2007.0077
651 Thorp, K.R., 2019. Long - term simulations of site - specific irrigation management for Arizona
652 cotton production. Irrig. Sci. https://doi.org/10.1007/s00271-019-00650-6
653 Toureiro, C., Serralheiro, R., Shahidian, S., Sousa, A., 2017. Irrigation management with remote
654 sensing: Evaluating irrigation requirement for maize under Mediterranean climate
655 condition. Agric. Water Manag. 184, 211–220. https://doi.org/10.1016/j.agwat.2016.02.010
656 Twarakavi, N.K.C., Sakai, M., Šimůnek, J., 2009. An objective analysis of the dynamic nature of
657 field capacity. Water Resour. Res. 45, 1–9. https://doi.org/10.1029/2009WR007944
658 van Genuchten, M.T., 1980. A Closed-form Equation for Predicting Hydraulic Conductivity of
659 Unsaturated Soils. Soil Sci. Soc. Am. J.
660 https://doi.org/doi:10.2136/sssaj1980.03615995004400050002x
661 van Genuchten MTh, Leij FJ, Y.S., 1991. The RETC code for quantifying the hydraulic
662 functions of unsaturated soils. US Environ. Prot. Agency R. S. Kerr Environ. Res. Lab. Off.
663 Res. Dev. Ada, OK.
664 Vellidis, G., Liakos, V., Perry, C., Porter, W.M., Tucker, M.A., 2016. Irrigation Scheduling for
665 Cotton Using Soil Moisture Sensors, Smartphone Apps, and Traditional Methods 772–780.

Viña, A., Gitelson, D.C., Rundquist, G., Keydan, B., Leavitt, Schepers, J.S., 2004. Monitoring Maize (Zea mays L.) Phenology with Remote Sensing. Agron. J. 96, 1139–1147. https://doi.org/10.1007/978-1-4614-3103-9

West, H., Quinn, N., Horswell, M., White, P., 2018. Assessing vegetation response to soil moisture fluctuation under extreme drought using sentinel-2. Water (Switzerland) 10, 1–22. https://doi.org/10.3390/w10070838

Yang, Y., Wendroth, O., Walton, R.J., 2016. Temporal Dynamics and Stability of Spatial Soil Matric Potential in Two Land Use Systems. Vadose Zo. J. 15, 0. https://doi.org/10.2136/vzj2015.12.0157

Zhang, N., Wang, M., Wang, N., 2002. Precision agriculture*a worldwide overview Naiqian. Comput. Electron. Agric. 36, 113–132. https://doi.org/10.1111/j.1751-1097.1990.tb01731.x

Zurweller, B.A., Rowland, D.L., Mulvaney, M.J., Tillman, B.L., Migliaccio, K., Wright, D., Erickson, J., Payton, P., Vellidis, G., 2019. Optimizing cotton irrigation and nitrogen management using a soil water balance model and in-season nitrogen applications. Agric. Water Manag. 216, 306–314. https://doi.org/10.1016/j.agwat.2019.01.011

Figures:

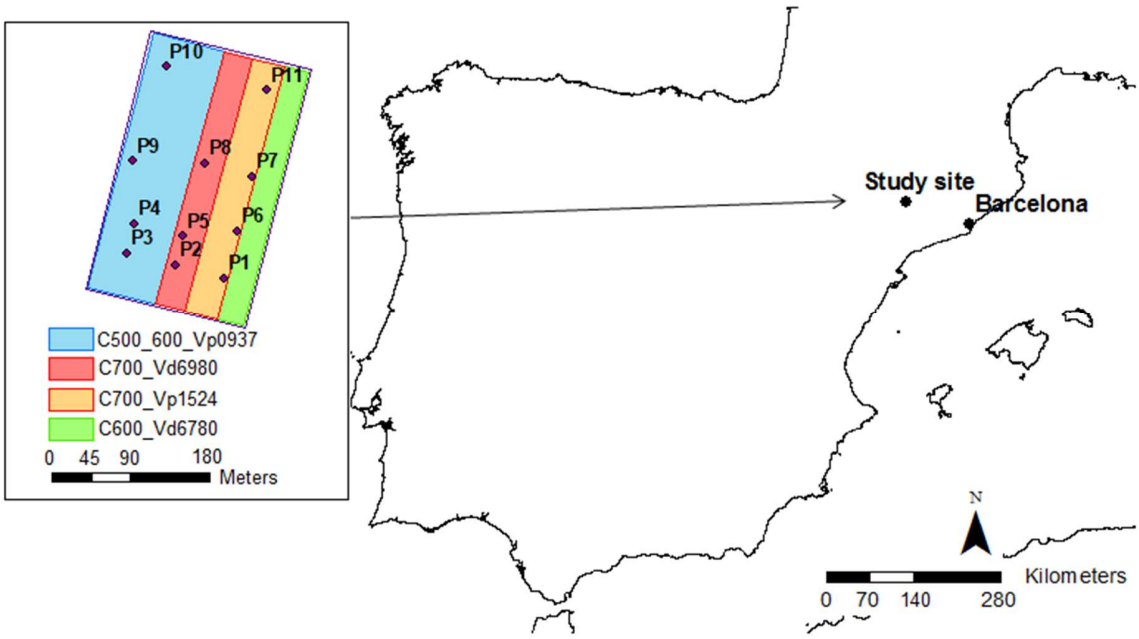

Figure 1. Study site location, soil moisture station locations, and maize variety plantings. The blue area represents maize variety p0937 (a combination of 500 and 600 series), the red area is variety d6980 (700 series), the yellow area is p1524 (700 series), and the green area is d6780 (600 series).

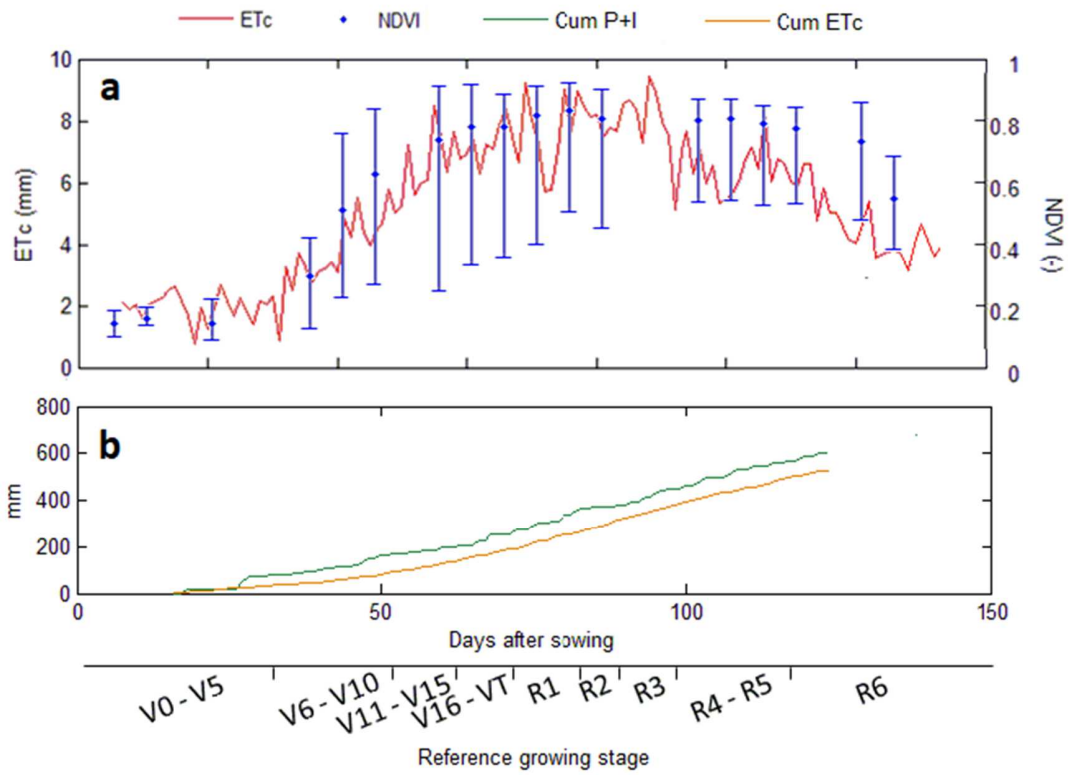

Figure 2. Field average evapotranspiration, NDVI, and cumulative water fluxes as a function of time and maize growth stage. The bars on the NDVI data indicate field maximum and minimum values. (V is vegetative stage; R is reproductive stage NDVI is Normalized Difference Vegetation Index; ETc is daily water requirements; Cum P+I is cumulative Precipitation and Irrigation; and Cum ETc is cumulative water requirements).

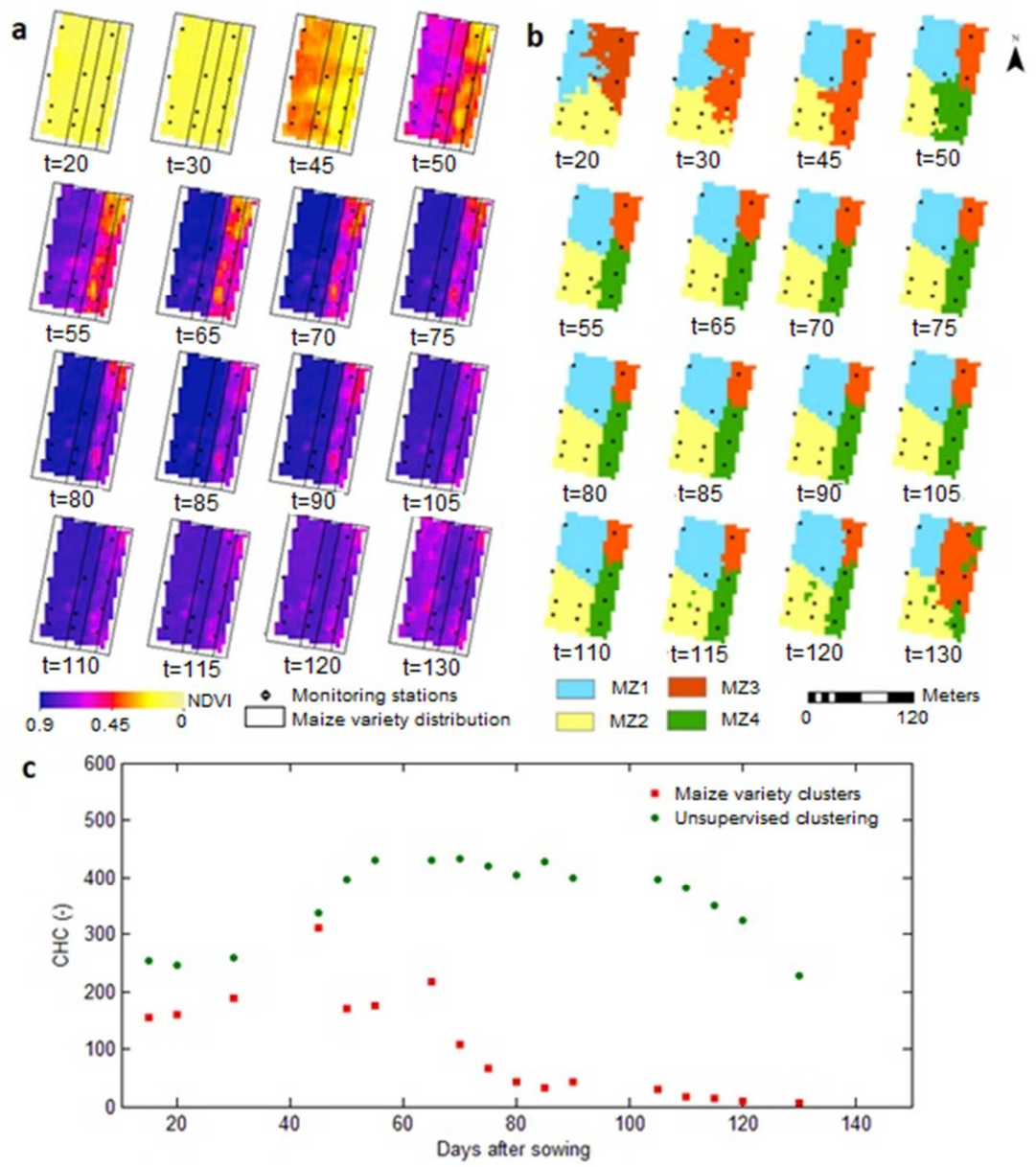

Figure 3. a) Normalized Difference Vegetation Index (NDVI) datasets measured by Sentinel 2 satellite through the growing season; b) dynamic management zone (MZ) delineation. The letter t indicates days after sowing; and c) Calinski-Harabaz criterion (CHC) for the NDVI grouped by maize variety (red squares) and with the unsupervised fuzzy-k clustering (green dots).

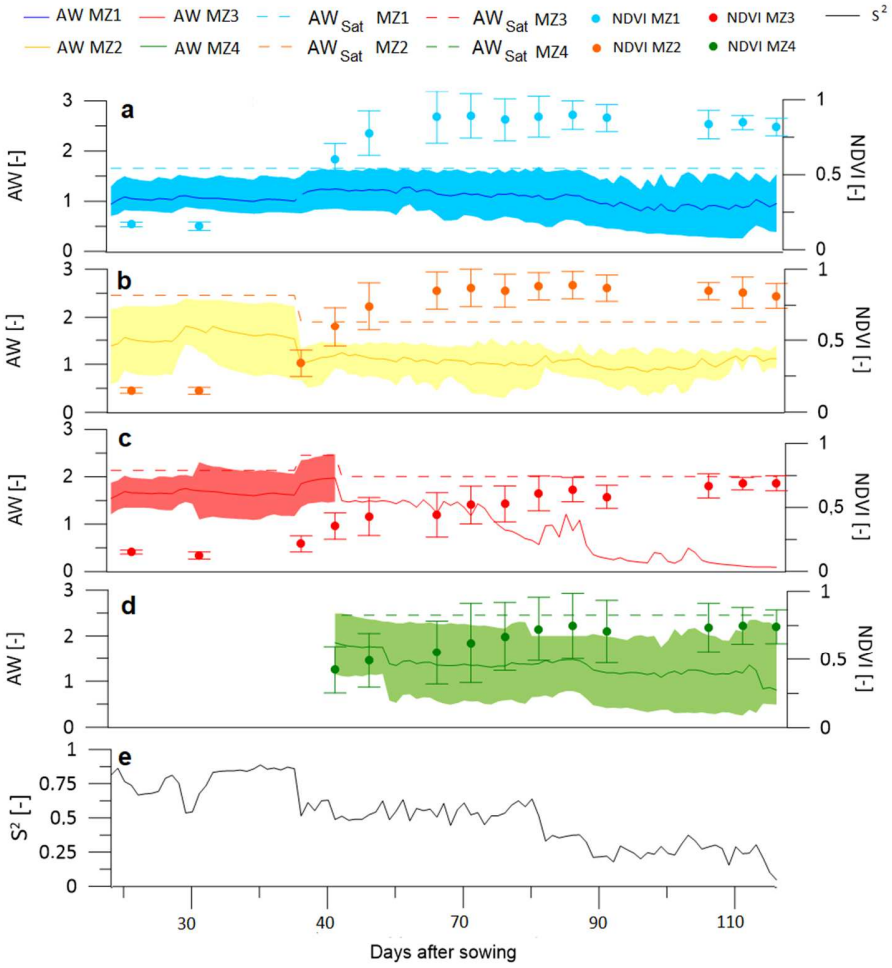

706

707 Figure 4. Soil profile available water (AW) and NDVI averages for a) MZ1, b) MZ2, c) MZ3,
708 d) MZ4. Shaded areas represent the maximum in minimum AW at each MZ, while dash lines show
709 available water saturated (AW_{sat}) (θ) and field capacity point (θ_{fc}). Error bars represents the
710 maximum and minimum NDVI at each MZ. Note that AW = 1 corresponds to a soil water content
711 equal to field capacity. Panel e) shows the daily total within-MZ weighted variance (S^2) of AW
712 relative to the daily field-wide AW variance (i.e., S^2=1).

713

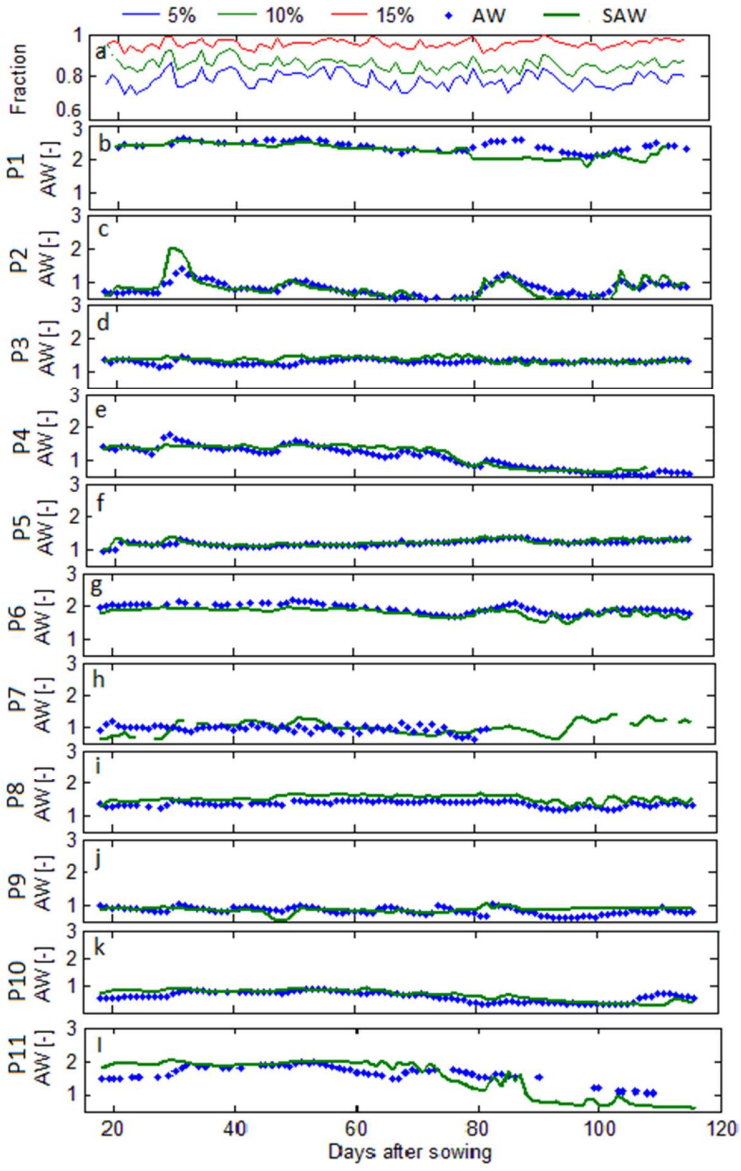

Figure 5. a) Evaluation of profile available water (AW) simulations showings the fraction of error greater than 5, 10, and 15%. b to l) Comparison between measured available water (AW) and simulated available water (SAW) at each station (P1 - P11).

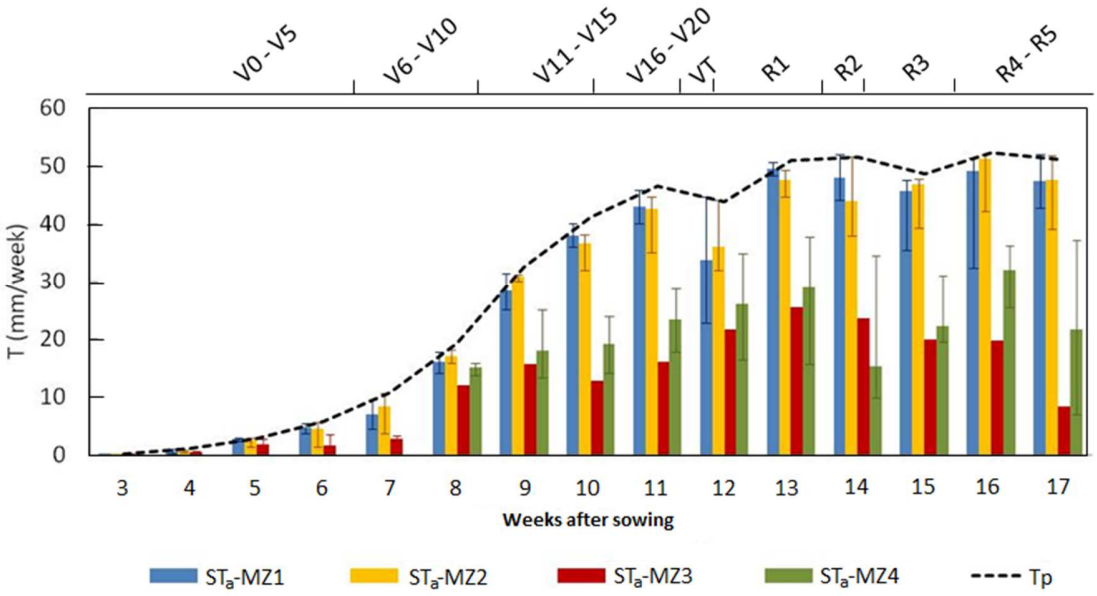

720

721 Figure 6. Simulated weekly transpiration at each MZ with the growing stages. Error bars

722 represent the maximum and minimum and the dash line shows the weekly potential transpiration.

723

Tables

Table 1. Soil samples texture, Organic Matter (OM) and bulk density (ρ_b) averages at each station.

Station	Depth (cm)	D<0.002 mm Clay (%)	0.002<D<0.02 mm Fine Silt (%)	0.02<D<0.05 mm Coarse Silt (%)	0.05<D<2 mm Sand (%)	OM (%)	ρ_b (gr/cm^3)
P1	0 - 5	36	27.3	13.8	22.9	1.18	1.66
	5 - 35	32	33.6	14.5	19.9	0.71	1.63
	35 - 60	26.5	28.1	9.7	35.7	0.5	1.68
P2	0 - 5	25.9	26.4	14.8	32.9	1.59	1.57
	5 - 35	25.2	26.1	15.1	33.6	1.1	1.58
	35 - 60	24.2	23.4	14.7	37.7	0.98	1.59
P3	0 - 5	36.5	32.1	14.5	16.9	0.7	1.54
	5 - 35	21.3	27.8	16.7	34.2	0.5	1.65
	35 - 60	24.4	31.8	8.3	35.9	0.65	1.60
P4	0 - 5	28.7	23.6	13.2	34.5	2.71	1.48
	5 - 35	28.5	28.9	11	31.6	1.02	1.59
	35 - 60	28.6	19.8	10.4	41.2	1.14	1.60
P5	0 - 5	22.5	26.3	15.6	35.6	0.57	1.56
	5 - 35	28.9	36.6	20.3	14.2	0.72	1.58
	35 - 60	21.8	28.9	7.3	42.0	0.42	1.56
P6	0 - 5	29.9	26.9	15.1	28.1	2.11	1.64
	5 - 35	29.3	25.7	14.9	30.1	0.85	1.67
	35 - 60	30.2	26	14.8	29.0	0.7	1.69
P7	0 - 5	28.1	36	17.1	18.8	3.14	1.65
	5 - 35	28	27.8	11.9	32.3	1.48	1.72
	35 - 60	27.2	24.3	14.3	34.2	1.27	1.69
P8	0 - 5	25.7	28.7	15.2	30.4	2.22	1.58
	5 - 35	27.7	26.1	14.7	31.5	1.5	1.64
	35 - 60	29.2	27.3	14.7	28.8	1.02	1.78
P9	0 - 5	23.7	26.1	14.8	35.4	2.48	1.53
	5 - 35	23.6	27.8	14.4	34.2	1.06	1.51
	35 - 60	23.5	27.7	14.8	34	0.99	1.51
P10	0 - 5	27.7	25.8	20.3	26.2	1.84	1.61
	5 - 35	28.3	29.5	19.2	26.0	0.72	1.62
	35 - 60	24.6	33.5	9.5	32.4	0.81	1.80
P11	0 - 5	29.4	35.9	14.9	19.8	0.73	1.63
	5 - 35	30.3	34.7	14.9	20.1	0.5	1.65
	35 - 60	26.1	30.5	16.4	27.0	0.5	1.64

728 Table 2. Soil hydraulic parameters from each station, where: θ_s is the saturated water content; θ_r is the residual water
729 content; α and n are shape parameters; K_s is the saturated hydraulic conductivity; θ_{fc} is simulated field capacity; and
730 θ_{wp} is wilting point. θ_s, θ_r and K_s parameters are fixed, while, α, n parameters are fitted.

Station	Depth (cm)	θ_s ($cm^3 \cdot cm^{-3}$)	θ_r ($cm^3 \cdot cm^{-3}$)	α (cm^{-1})	n (-)	K_s ($cm \cdot d^{-1}$)	θ_{fc} ($cm^3 \cdot cm^{-3}$)	θ_{wp} ($cm^3 \cdot cm^{-3}$)
P1	0 - 5	0.424	0.026	0.0169	1.140	2.05	0.345	0.196
	5 – 35	0.407	0.027	0.0150	1.141	2.52	0.351	0.190
	35 - 60	0.364	0.037	0.0115	1.232	1.00	0.350	0.110
P2	0 - 5	0.389	0.061	0.0126	1.364	2.95	0.270	0.103
	5 – 35	0.388	0.060	0.0130	1.358	2.94	0.265	0.104
	35 - 60	0.321	0.047	0.0242	1.354	1.53	0.290	0.124
P3	0 - 5	0.418	0.012	0.0103	1.313	4.42	0.330	0.085
	5 – 35	0.362	0.025	0.0101	1.329	5.63	0.273	0.070
	35 - 60	0.341	0.017	0.0083	1.345	11.47	0.261	0.066
P4	0 - 5	0.439	0.024	0.0658	1.301	5.70	0.340	0.187
	5 – 35	0.400	0.031	0.0143	1.290	4.60	0.300	0.192
	35 - 60	0.395	0.018	0.0424	1.315	4.90	0.315	0.181
P5	0 - 5	0.450	0.062	0.0099	1.497	6.88	0.340	0.070
	5 – 35	0.460	0.067	0.0094	1.402	1.94	0.340	0.080
	35 - 60	-	-	-	-	-	-	-
P6	0 - 5	0.420	0.030	0.0126	1.153	12.00	0.371	0.172
	5 – 35	0.430	0.050	0.0828	1.154	9.40	0.390	0.198
	35 - 60	0.421	0.010	0.0974	1.146	8.10	0.390	0.182
P7	0 - 5	0.375	0.024	0.0105	1.118	1.06	0.300	0.208
	5 – 35	0.349	0.026	0.0380	1.141	3.34	0.300	0.196
	35 - 60	0.361	0.049	0.0391	1.141	4.10	0.280	0.107
P8	0 - 5	0.402	0.040	0.0135	1.375	4.01	0.310	0.123
	5 – 35	0.379	0.030	0.0115	1.356	3.05	0.280	0.090
	35 - 60	0.328	0.020	0.0121	1.287	1.75	0.280	0.080
P9	0 - 5	0.420	0.060	0.0105	1.462	5.79	0.300	0.089
	5 – 35	0.430	0.060	0.0107	1.441	4.70	0.330	0.091
	35 - 60	0.430	0.060	0.0109	1.433	5.52	0.330	0.090
P10	0 - 5	0.389	0.073	0.0115	1.421	3.98	0.301	0.105
	5 – 35	0.387	0.072	0.0112	1.425	4.56	0.300	0.080
	35 - 60	0.320	0.058	0.0181	1.256	1.87	0.290	0.090
P11	0 - 5	0.400	0.012	0.0784	1.121	10.00	0.380	0.188
	5 – 35	0.451	0.018	0.0308	1.141	5.27	0.375	0.188
	35 - 60	0.420	0.014	0.0121	1.112	11.00	0.350	0.250

731
732

733 Table 3. Periods where one or more stations change MZ membership.

Period (Day after sowing)	MZ1	MZ2	MZ3	MZ4
Period 1 (19-29)	P8, P9, P10	P1, P2, P3, P4, P5, P6	P7, P11	-
Period 2 (30-44)	P8, P9, P10	P1, P2, P3, P4, P5	P6, P7, P11	-
Period 3 (45-49)	P8, P10	P2, P3, P4, P5, P9	P1, P6, P7, P11	-
Period 4 (50-54)	P8, P10	P2, P3, P4, P9	P7, P11	P1, P5, P6
Period 5 (55-115)	P8, P10	P2, P3, P4, P5, P9	P11	P1, P6, P7

734

Table 4. Irrigation scheduling calendar based on growing stages and MZs distribution. h_{th}, is the possible pressure head threshold (the optimal pressure head threshold in bold); *I,* is the irrigation required to achieve maximized transpiration; τ, is the irrigation duration; Z_{tr}, is the trigger soil depth. Optimal irrigation parameters representing the optimal irrigation strategy is represented in bold.

		V0-V5		**V6-V10**		**V11-V15**		**VT**		**R1-R6**	
		Trigger Depth = 10 cm		**Trigger Depth = 20cm**		**Trigger Depth = 20 cm**		**Trigger Depth = 40 cm**		**Trigger Depth = 40 cm**	
	h_{th} (kPa)	**Irrig. Required (mm)**	**τ (h)**	**Irrig. Required (mm)**	**τ (h)**	**Irrig. Required (mm)**	**τ (h)**	**Irrig. Required (mm)**	**τ (h)**	**Irrig. Required (mm)**	**τ (h)**
MZ1	**0**	-	-	-	-	-	-	-	-	-	-
	-10	-	-	-	-	-	-	-	-	-	-
	-20	-	-	-	-	-	-	-	-	-	-
	-23.3	-	-	**12.5**	**1.9**	-	-	-	-	-	-
	-26.7	**13.1**	**2.0**	13.5	2.1	-	-	-	-	-	-
	-30	14.0	2.2	14.1	2.2	**19.0**	**2.9**	**15.0**	**2.3**	**17.0**	**2.6**
	-40	15.0	2.3	14.5	2.2	21.0	3.2	17.0	2.6	21.0	3.2
	-60	16.0	2.5	18.5	2.8	25.0	3.8	23.0	3.5	29.0	4.5
	-100	17.1	2.6	22.5	3.5	29.0	4.5	33.0	5.1	45.0	6.9

	h_{th} (kPa)	**Irrig. Required (mm)**	**τ (h)**	**Irrig. Required (mm)**	**τ (h)**	**Irrig. Required (mm)**	**τ (h)**	**Irrig. Required (mm)**	**τ (h)**	**Irrig. Required (mm)**	**τ (h)**
MZ2	**0**	-	-	-	-	-	-	-	-	-	-
	-10	-	-	-	-	-	-	-	-	-	-
	-18.3	**12.4**	**1.9**	-	-	-	-	-	-	-	-
	-20	12.4	1.9	-	-	-	-	-	-	-	-
	-24	12.9	2.0	**15.3**	**2.4**	-	-	-	-	-	-
	-30	13.9	2.1	18.3	2.8	**13.0**	**2.0**	**13.0**	**2.0**	**13.0**	**2.0**
	-40	14.4	2.2	19.3	3.0	18.0	2.8	23.0	3.5	23.0	3.5
	-60	16.9	2.6	24.3	3.7	23.0	3.5	33.0	5.1	33.0	5.1
	-100	19.9	3.1	30.3	4.7	29.0	4.5	45.0	6.9	45.0	6.9

	h_{th} (kPa)	Irrig. Required (mm)	τ (h)	Irrig. Required (mm)	τ (h)	Irrig. Required (mm)	τ (h)	Irrig. Required (mm)	τ (h)	Irrig. Required (mm)	τ (h)
MZ3	**0**	-	-	-	-	-	-	-	-	-	-
	-10	-	-	**13.0**	**2.0**	**13.0**	**2.0**	**13.0**	**2.0**	**13.0**	**2.0**
	-20	**13.0**	**2.0**	17.0	2.6	17.0	2.6	21.0	3.2	21.0	3.2
	-30	15.0	2.3	21.0	3.2	21.0	3.2	29.0	4.5	29.0	4.5
	-40	16.0	2.5	23.0	3.5	23.0	3.5	33.0	5.1	33.0	5.1
	-60	18.0	2.8	27.0	4.2	27.0	4.2	41.0	6.3	41.0	6.3
	-100	20.5	3.2	28.0	4.3	28.0	4.3	43.0	6.6	43.0	6.6

	h_{th} (kPa)	Irrig. Required (mm)	τ (h)	Irrig. Required (mm)	τ (h)	Irrig. Required (mm)	τ (h)	Irrig. Required (mm)	τ (h)	Irrig. Required (mm)	τ (h)
MZ4	**0**	-	-	-	-	-	-	-	-	-	-
	-10	-	-	-	-	-	-	**13.0**	**2.0**	**13.0**	**2.0**
	-16.7	-	-	-	-	**15.0**	**2.3**	15.0	2.3	15.0	2.3
	-20	-	-	-	-	16.0	2.5	17.0	2.6	17.0	2.6
	-30	-	-	-	-	19.0	2.9	25.0	3.8	25.0	3.8
	-40	-	-	-	-	21.0	3.2	29.0	4.5	29.0	4.5
	-60	-	-	-	-	23.0	3.5	33.0	5.1	33.0	5.1
	-100	-	-	-	-	29.0	4.5	45.0	6.9	45.0	6.9

738

739 Table 5. Comparisons of optimal actual transpiration (OpT_a), optimal water applied ($OpIA$), simulated actual
740 transpiration (ST_a), and simulated water applied (SAI).

	OpT_a (mm)	$(OpT_a - ST_a)/ST_a$ (%)	$OpIA$ (mm)	$(OpIA - SAI)/SAI$ (%)
MZ1	405.6	8.0	525.5	-11.0
MZ2	405.6	4.8	517.8	-12.8
MZ3	107.5	23.9	217.5	-28.5
MZ4	271.7	52.6	350.2	-16.6

741

742

Appendix A. Supplementary data

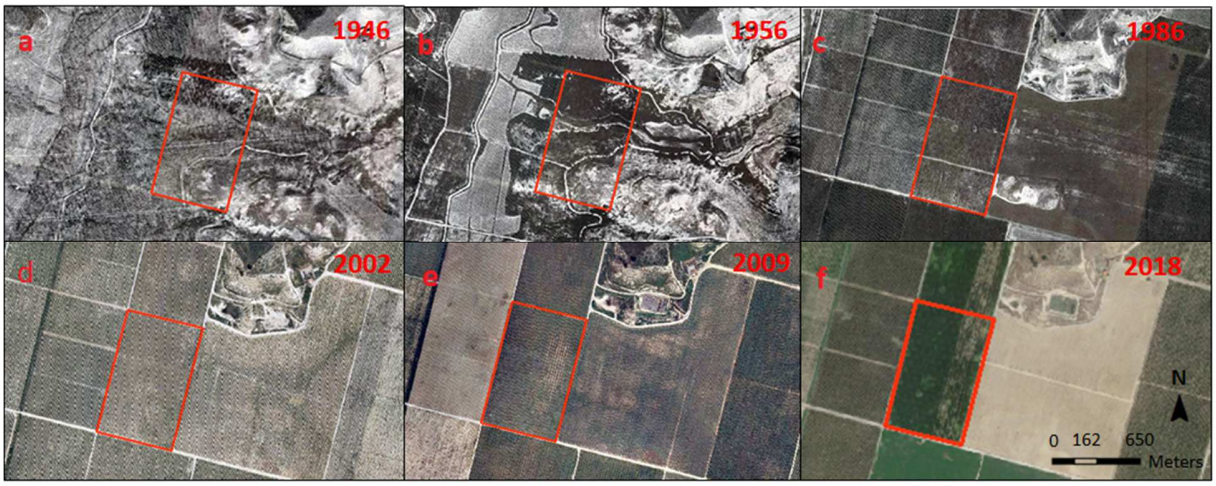

Figure A.1. Historical land use and topography modifications at the study site.

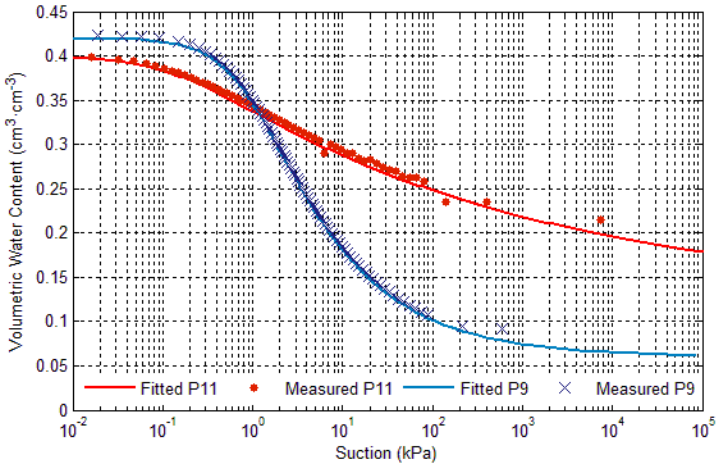

Figure A.2. Soil water retention curves at 10 cm depth from two stations located on opposite edges of the filed. Station P9 is located on the west side and P11 on the east.

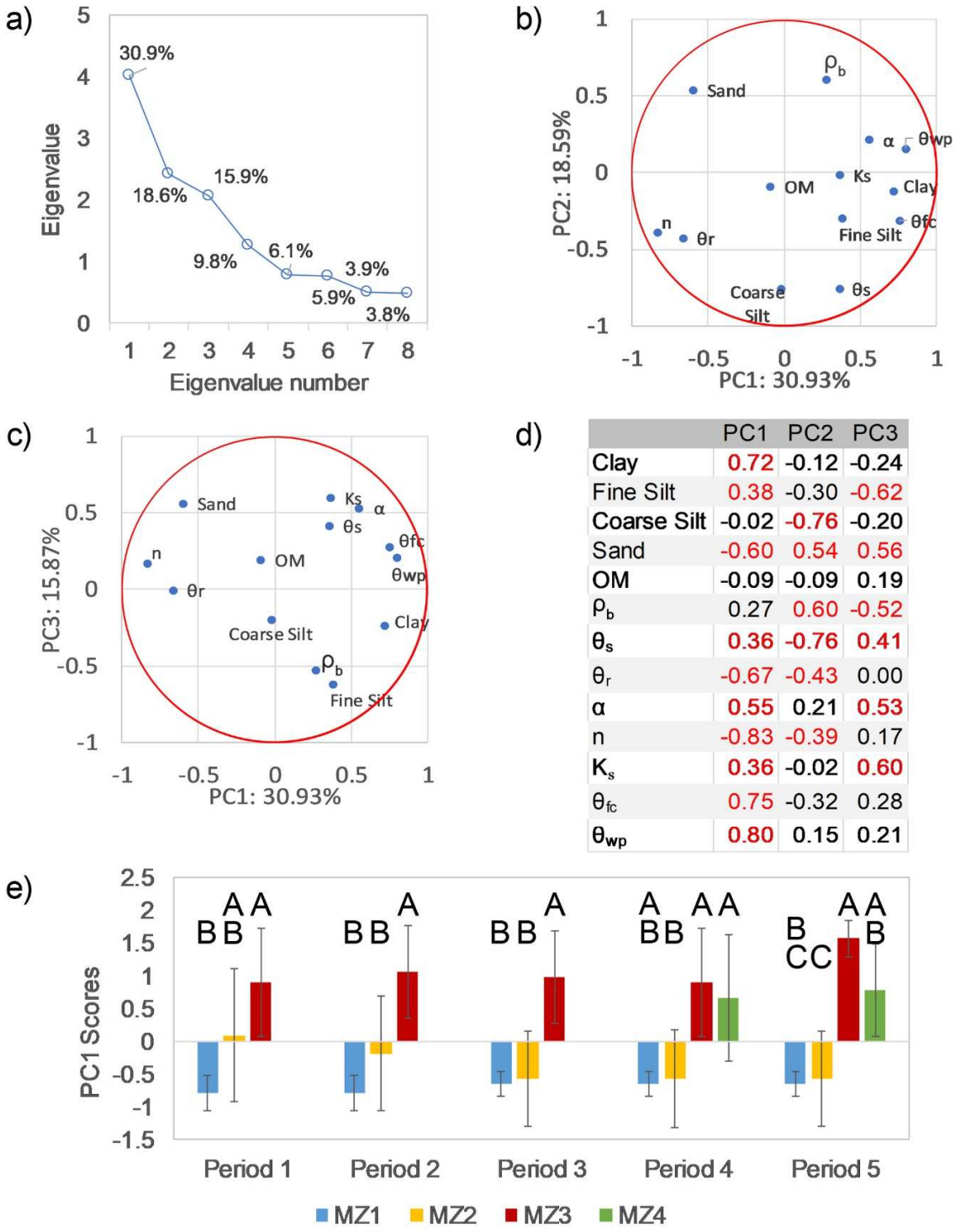

	PC1	PC2	PC3
Clay	0.72	-0.12	-0.24
Fine Silt	0.38	-0.30	-0.62
Coarse Silt	-0.02	-0.76	-0.20
Sand	-0.60	0.54	0.56
OM	-0.09	-0.09	0.19
ρ_b	0.27	0.60	-0.52
θ_s	0.36	-0.76	0.41
θ_r	-0.67	-0.43	0.00
α	0.55	0.21	0.53
n	-0.83	-0.39	0.17
K_s	0.36	-0.02	0.60
θ_{fc}	0.75	-0.32	0.28
θ_{wp}	0.80	0.15	0.21

753

754 Figure A.3. a) Eigenvalue and percent of variance explained by the first eight components of the

755 principal component (PC) analysis; b) bi-plot of select soil properties (clay, fine silt, coarse silt,

sand, and organic matter (OM) content; bulk density (ρ_b); water content at saturation (θ_s); residual water content (θ_r); water content at field capacity (θ_{fc}); water content at wilting point (θ_{wp}); saturated hydraulic conductivity (K_s); and shape parameters α and n) for PC1 and PC2; c) same for PC1 and PC3; d) Pearson correlation matrix for the first three PCs and selected soil properties (significant ($p<0.05$) correlations highlighted in red); and e) averages (bars) and standard deviations (lines) ofPC1 for the four management zones (MZs) through the growing season. Capital letters indicate significant ($p<0.05$) differences within MZs according to the Kruskal-Wallis test.